AIMS Geosciences

AIMS Geosciences, 6(2): 231–257.
DOI: 10.3934/geosci.2020014
Received: 09 April 2020
Accepted: 11 June 2020
Published: 22 June 2020

http://www.aimspress.com/journal/geosciences

Research article

Evaluation of open Digital Elevation Models: estimation of topographic indices relevant to erosion risk in the Wadi M'Goun watershed, Morocco

Maryam Khal[1,*], Abdellah Algouti[1], Ahmed Algouti[1], Nadia Akdim[2], Sergey A. Stankevich[3] and Massimo Menenti[4,5]

[1] Cadi Ayyad University, Faculty of Sciences, Department of Geology, Laboratory of Geosciences, Geotourism, Natural Hazards and Remote Sensing, Bd. BO 2390, 40000 Marrakech, Morocco
[2] Department of Geology, Faculty of Sciences, Chouaib Doukkali University, Route Ben Maachou, B.P 20, 24000, El Jadida, Morocco
[3] Scientific Centre for Aerospace Research of the Earth, NAS of Ukraine, 55-B O. Gonchar str., Kiev, 01054, Ukraine
[4] Geosciences and Remote Sensing Department, Delft University of Technology, Stevinweg 12628 CN Delft, The Netherlands
[5] State Key Laboratory of Remote Sensing Science, Institute of Remote Sensing and Digital Earth, Chinese Academy of Sciences, Beijing 100101, China

*** Correspondence:** Email: Maryam.khal@ced.uca.ma; Tel.: +212655918913.

Abstract: Various Global Digital Elevation Models (DEM) are available freely on the Web. The main objective of this work is to evaluate the latest digital elevation models towards the estimation of morphological and topographic erosion parameters in the Wadi M'Goun watershed. We have evaluated multiple DEMs: SRTM (3-arcsec resolution, 90 m), ASTER GDEM (1-arcsec resolution, 30 m), SRTMGL1 V003 (30 m), and ALOS-PALSAR (12.5 m). We have applied for this purpose open source GIS software. To compare and evaluate each DEM, different processing methods have been applied to estimate the Wadi M'Goun watershed characteristics, namely Hypsometry, topographic slope extraction, retrieval of Slope Length and Steepness factor (LS-factor) and topographic wetness index. The accuracy of the ALOS-PALSAR and SRTMGL1 V003 (30 m) DEMs met the requirements applying to the required morphometric parameters. DEMs vertical accuracy has been evaluated by applying the root mean square error (RMSE) metric to DEM

elevations vs. actual heights of 353 sample points extracted from an accurate survey-based map (toposheet). The RMSE was 1718 mm for ALOS-PALSAR, 1736 for SRTM 1-arcsec, 1958 for ASTER GDEM 1-arcsec and, 3189 for SRTM 3-arcsec. These results indicate that best accuracy is achieved with the high-resolution of the ALOS PALSAR DEM. This study suggests potential uncertainties in the open-source DEMs, which should be taken into account when estimating topographical and morphometric parameters related to erosion risk in the Wadi M'Goun watershed.

Keywords: erosion risk; open DEM; SRTM; ASTER GDEM; SRTMGL1 V003; ALOS-PALSAR; M'Goun watershed; Central High Atlas

1. Introduction

Accurate digital elevation models (DEM) provide critical information from both a scientific and a socio-economic point of view. Digital elevation models (DEM) play a crucial role in the estimation of geophysical variables, e.g. gravity field modeling, geology, geomorphological characterization of watersheds, drainage characteristics, soil erosion rate estimation, and assessment of surface runoff and recharge [1–4]. Moreover, reliable topographic information carries multiple societal benefits, e.g. for precise flood prediction and management [5,6] or local-scale weather forecasts [7]. Morphometric characteristics and topographic parameters in Moroccan High Atlas watersheds are relevant to improve the performance of the agricultural sector, since data on elevation are needed to assess e.g. siltation of reservoirs and soil degradation.

DEMs are needed to estimate topographic characteristics of watersheds such as: slope length, hypsometry, channel network, Topographic Wetness Index, relative relief, drainage density [8–10]. The quality of a DEM is affected by different types of errors and changes with terrain conditions [11]. The accuracy of the DEMs influences directly the quality of studies on watersheds [12].

Various DEMs are available at different resolutions and generated by different methods [13–16]. DEMs which provide good terrain representation have a very high price as a starting point for further analysis. Currently, some of the DEMs have been rendered using remote sensing techniques: these are easily accessible and open source with good accuracy even compared with proprietary DEMs. Examples of open-source DEMs are: the Shuttle Radar Topography Mission (SRTM) in 2000, the Advanced Spaceborne Thermal Emission and Reflection Radiometer (ASTER) Global Digital Elevation Model (GDEM) in 2009, and the Advanced Land Observing Satellite Phased Array Type L-band Synthetic Aperture Radar (ALOS PALSAR) in 2006, specifically addressed in this comparative study. Accuracy of DEMs needs to be documented to provide users with the information needed to assess the reliability of estimated watershed characteristics. Different DEMs have different accuracy, thus affecting the hydrologic analyses of watersheds [17–19]. A slight variation in estimated hydrological characteristics results in a very large difference in estimated drainage for relatively small catchments. Multiple studies documented the severe impacts of inaccurate DEMs [20–22].

Several authors focused on the accuracy assessment of DEMs, e.g. [23–28]. The paper [29] evaluated the slope estimates based on the SRTM DEM against those estimated by interpolating topographic contours. The paper [30] evaluated the uncertainty of soil erosion estimated using the MUSLE model [31] in relation with the accuracy of the ASTER 30 m and SRTM 90 m DEMs. The paper [32] evaluated the accuracy of the Advanced Spaceborne Thermal Emission Reflectometer

Global DEM (ASTER GDEM2) and two DEMs based on the Shuttle Radar Topography Mission (SRTM) over the Australian continent. Researchers have also used high-resolution DEMs to measure soil erosion using the RUSLE model [33] i.e. the GTOPO30, SRTM, ASTER, and CARTOSAT DEMs [34–36]. These studies show that current understanding of the uncertainty of various DEMs is not sufficient and the impact on the extraction of watershed geomorphologic characteristics and on the estimation of erosion risk should be evaluated in more detail.

In work [37] a valuable method is described to evaluate the impact of DEM quality on the assessment of natural hazard risk. The quality is assessed by taking into account DEM usability and by its representational, qualitative, and intrinsic features.

The main objective of this study is to evaluate the accuracy of four open source DEMs having different spatial resolution, namely SRTM 3-arcsec (90 meters), DEM SRTM 1-arcsec (30 meters), ASTER GDEM 1-arcsec resolution (30 meters) and ALOS PALSAR (L-band 24 cm wavelength, 12.5 meters resolution). The evaluation was focused on the estimation of the morphometric parameters required to assess the vulnerability to water erosion of the Wadi M'Goun watershed. The vertical accuracy of DEMs has been evaluated using actual heights of the sample points extracted from an accurate map (toposheet), after converting height data to the same datum.

2. Materials and method

2.1. Study area

The M'Goun watershed is located in the southern flank of Central High Atlas and belongs to the upper Draa Basin. It is located a hundred kilometers north-east of Ouarzazate and is bordering the Kelaat M'Gouna municipality and the valley of Boumalne Dades (Figure 1). The latitudinal and longitudinal boundaries of the area are 31°20′ and 31°40′N and 6° and 6°30′W and the basin includes one of the highest peaks of North Africa: Ighil n'Mgoun (4071 m). The climate of the M'Goun valley is semi-arid to subhumid, dry in summer and rainy in winter and spring. In the upper catchment, most of the precipitation is in the form of snow. The flows are of torrential type with severe rainfall events, leading to frequent floods in the alluvial plains. In this context, water erosion triggers landslides, gullying, stripping of soil and shorelines, and the destruction of infrastructure (bridges and roads).

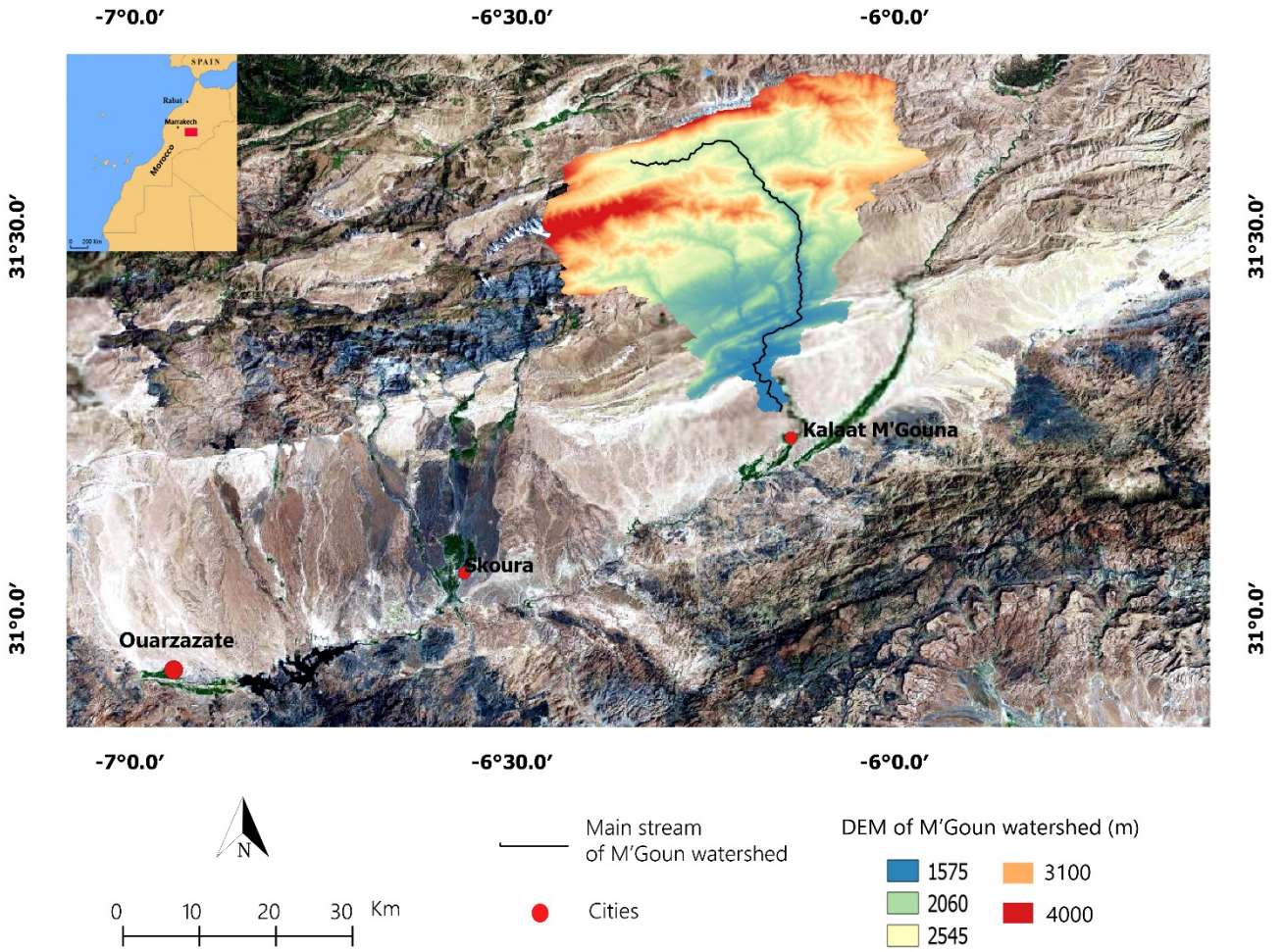

Figure 1. Geographic situation of M'Goun watershed: Satellite image of the southern flank of Central High Atlas; elevation is the DEM ALOS-PALSAR 12.5 m (Source: SAS Planet, 2018).

2.2. Workflow

In this research, four open source DEMs with different precision and coverage were acquired and tested to assess the impact of their accuracy when estimating the M'Goun watershed characteristics. The software used was all open source: Saga GIS and QGIS.

The approach briefly described in the Introduction leads to the workflow in Figure 2, which shows how the DEMs accuracy is assessed, then applied to retrieve the morphometric and topographic parameters required to estimate the rate of water erosion in the M'Goun watershed.

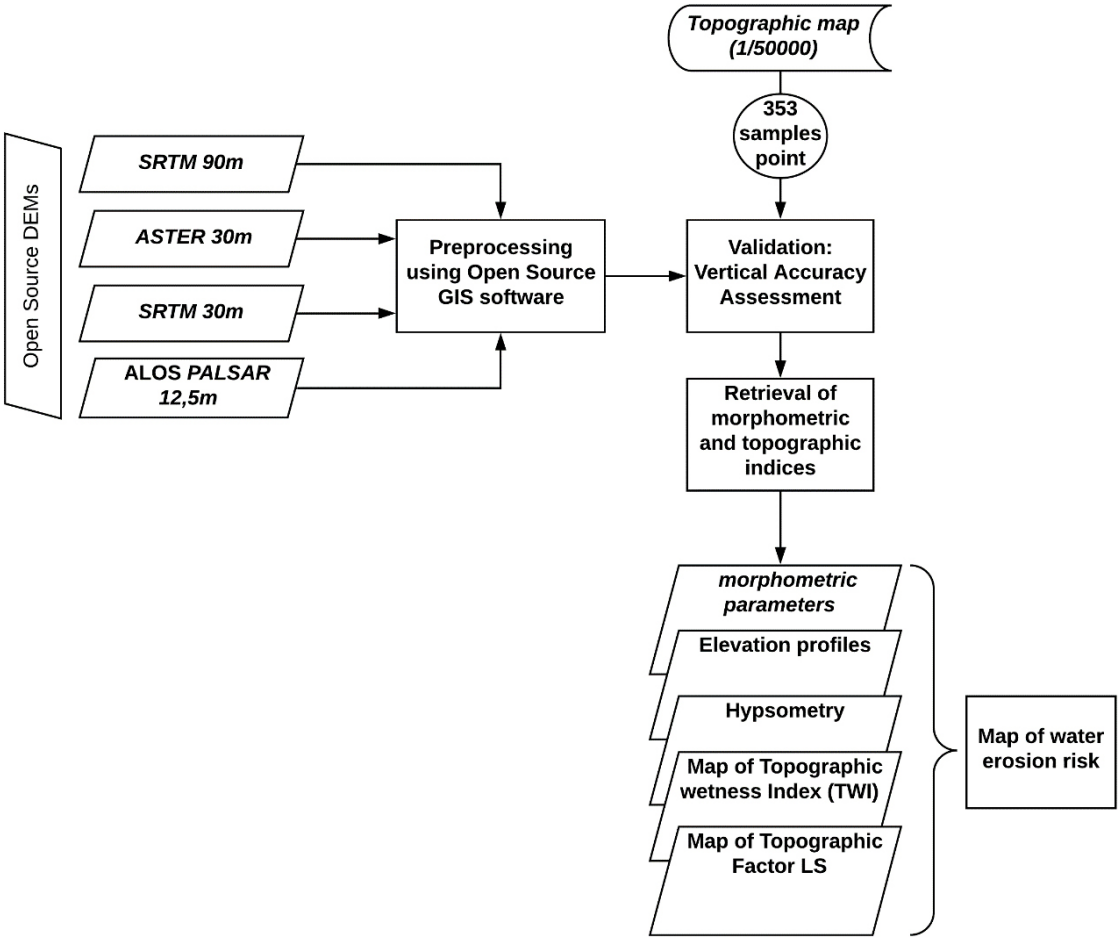

Figure 2. Workflow of the applied methodology.

2.3. Description of DEM used

The specific characteristics of the datasets are:

There are two SRTM DEM data products: SRTM 3-arcsec and SRTM 1-arcsec, with the spatial resolution of 90 m and 30 m, respectively. The SRTM DEMs products used are downloaded via U.S. Geological Survey (USGS) EarthExplorer web-platform (https://earthexplorer.usgs.gov/).

The Shuttle Radar Topography Mission (SRTM) refers to topographic and matrix files provided by two US agencies, the National Imagery and Mapping Agency (NIMA) and the National Aeronautics and Space Administration (NASA). These altimetry data were collected during 11 days in February 2000 using a space-borne dual imaging radar (SIR-C) and a dual-band synthetic aperture radar (X-SAR). From these data a DEM was generated that covers the Earth between 60°N and 56°S [38]. One DEM dataset has a resolution of 1 arc-second (30 m near the equator) (SRTM1), and the other has a resolution of 3 arc-seconds (90 m near the equator) (SRTM3) [38]. Those items have been made available in 2003 by the United States Geological Survey [38] and they have been freely accessible to the public since September 2003.

Advanced Spaceborne Thermal Emission and Reflection Radiometer (ASTER) is an advanced multispectral imaging device that started aboard NASA TERRA satellite in December 1999. The product ASTER DEM is yielded using the images band 3N (Nadir view) and band 3B (Backward view) of an ASTER level-1A image acquired in the Visible and Near Infrared (VNIR) bands. The VNIR subsystem contains two sets of separate telescopes to help acquire stereoscopic data.

ASTER Global Digital Elevation Model (ASTER GDEM) is a project that was launched on June 29th, 2009, in the framework of the collaboration between the National Aeronautics and Space Administration (NASA) and Japan Ministry of Economy, Trade and Industry (METI). The Advanced Space Thermal Emission Radiometer (ASTER) collected about 1,200,000 scenes of stereoscopic data. The DEM GDEM version 1 (GDEM v1) was developed using these data. This free version has a horizontal resolution of 1 arc second (30 m near the equator) covering 99% of the land area. In October 2011, version 2 of GDEM was released, improved over the previous version as regards the filling of voids.

ALOS-PALSAR (**Advanced Land Observing Satellite Phased Array L-band Synthetic Aperture Radar**) was launched on 2006 by the Japan Aerospace and Exploration Agency (JAXA). The ALOS-PALSAR was operational until May 12, 2011. The satellite has provided Earth observation data with high resolution for topographic mapping, disaster and environmental surveillance, and climate change investigation. ALOS was launched in a sun-synchronous orbit and circled around the Earth every 100 minutes, 14 times a day. ALOS-PALSAR returned to the original path (repetition cycle) every 46 days. The inter-orbit distance was about 59.7 km at the equator. ALOS-PALSAR has a spatial resolution of 12.5 m at 23.62 cm (1.27 GHz) wavelength with HV polarization and angle of incidence 38.7°.

2.4. DEMs preprocessing

The data used for this study were downloaded via NASA Earthdata web-service (https://earthdata.nasa.gov/) at different spatial resolutions. The four DEMs were transformed into the same projection system UTM, zone 29 north, WGS84 ellipsoid was selected for both datum and spheroid. The SAGA Module Fill Sinks, which applies the algorithm proposed by [39], was used to identify and fill surface depressions in the DEMs.

2.4.1. Geoid correction of ALOS-PALSAR DEM

The raw ALOS-PALSAR DEM elevation shows a difference in topographic height compared to a topographic map [40]. These data require a geoid correction with a method that consists in determining by GPS the ellipsoidal height of some benchmarks (h) and leveling the altitude at the same points (H) (Figure 3) [41]. The geoid height above the ellipsoid, *N*, is sometimes called geoid undulation. It can be used to convert a height above the ellipsoid, *h*, to the corresponding height above the geoid (the orthometric height, approximately the height above mean sea level), *H*, using the equations below:

$$H = h - N \tag{1}$$

In our study area, the estimated geoid height (*N*) is 50 m, calculated online using GeoidEval utility (https://geographiclib.sourceforge.io/cgi-bin/GeoidEval).

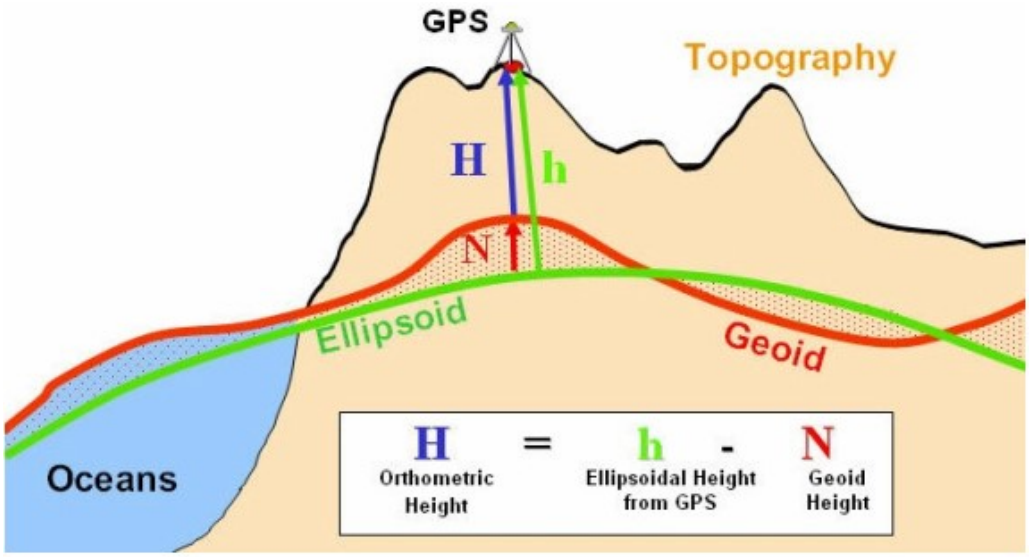

Figure 3. Cartoon showing the ellipsoid, geoid, and topographic surface (topography of landmass as well as bathymetry of oceans). *H* is the elevation above the geoid, *h*—height of the ellipsoid, and *N* is the height of the geoid (undulation) above the ellipsoid [41].

2.5. DEMs vertical accuracy

DEMs vertical accuracy has been assessed using a method of random points generation. A total of 353 sample points of actual heights were collected from the planimetric survey-based map (toposheet). We have used two topographic maps to cover the study area, i.e. the Tabant and Tignatine topographic maps, both at 1:50000 scale. The topographic maps were georeferenced using UTM projection system, zone 29 north, WGS84 ellipsoid.

The ground truth data extracted from the toposheet was analyzed as regards the positioning accuracy by comparing actual heights with the corresponding DEMs heights. The DEMs vertical accuracy was evaluated by applying different metrics: mean error ($Mean_{error}$), Sample Variance (σ^2), standard deviation error (σ) and root mean square error (*RMSE*) used in [42,43].

2.6. Retrieval of morphometric and topographic parameters

2.6.1. Morphometric parameters

The data used for this study are at different spatial resolutions. The delineation of Wadi M'Goun watershed has been based on thematic layers such as fill, flow direction, flow accumulation, stream to feature, etc. These thematic layers are generated for each DEM and processed using the Hydrology SAGA-GIS Tool. Then the attribute Table, containing stream length, basin area, basin perimeter, basin relief, etc., has been generated and other morphometric parameters have been computed as detailed below.

Altitude:

The different altitudes of the catchment, including minimum and maximum, have been acquired as the first point from toposheet maps. The maximum elevation corresponds to the highest point of the watershed, and the minimum elevation corresponds to the lowest point, this is typically the catchment outlet area. These values define a watershed's altimeter amplitude and help calculate the mean slope. The mean altitude of the watershed can be calculated [44] as:

$$Ha = \sum \frac{A_{i,i+1}(h_i + h_{i+1})}{2A} \tag{2}$$

where Ha is the mean elevation of the catchment (m); $A_{i;i+1}$ is the area between two consecutive contour lines (km^2); h_i; h_{i+1} is the altitude of the contour line (m); A is the catchment area (km^2).

Stream length:

The total length of particular stream segments of each order is that order's stream length. The length of the stream measures the mean length of a stream in each order and is calculated by dividing the total length of all streams by the number of streams in that order [45]:

$$Lu = L1 + L2 + \cdots + Ln \tag{3}$$

Mean Stream Length Ratio:

$$RI = \frac{Lu}{L(u-1)} \tag{4}$$

where Lu is overall stream length of the order "u", and $L(u-1)$ is overall stream length of its following lower order.

Concentration time:

In the watershed, the water concentration-time is defined as the maximum time for a drop of water falling on the surface of the watershed to reach the downstream boundary of the catchment [46]. The concentration-time t_c, therefore, corresponds to the maximum sum of the three elements using empirical formulas [47]:

$$t_c = max \sum (t_h + t_r + t_a) \tag{5}$$

where t_h is the humidification time, t_r is the runoff time and ta is the moving time.

Watershed shape (Equivalent rectangle):

The notion of the equivalent rectangle was introduced by [48] to make it easy to compare watersheds with each other as regards the influence of their characteristics on the flow.

Orographic coefficient:

There exist four different systems of ordering streams [49,50]. The system of Strahler slightly modified the Horton's system and is more used due to its simplicity.

Massivity coefficient:

The massivity coefficient (*Cm*) is an indicator of increments in slope as elevation increases. The *Cm* index reflects also erosion-prone basins. The Cm represents the relationship between the average height of the watershed and its area, which is expressed as a percentage. Small values of the coefficient of massivity correspond to watersheds with very high relief, while large values of the

coefficient reflect watersheds with moderate relief [51]. The massivity coefficient of the watershed can be calculated with the following relation [45]:

$$Cm = \frac{\overline{H}}{A} \tag{6}$$

with $\overline{H}$ is the mean basin elevation and *A* is the area.

2.6.2. Topographic indices

The topographical indices relevant to the erosion risk namely elevation, slope, topographic wetness index and topographic factor LS have been computed using the SAGA-GIS Terrain Analysis Tool. Then, they have been compared for four digital elevation models to assess the effect of DEM accuracy on the assessed water erosion risk.

The average elevation of a watershed is determined directly from the hypsometric curve. The mean altitude of a catchment is also used for determining particular hydro-meteorological parameters and complements the field knowledge on the terrain and the delineation of major geomorphic features, such as drainage systems and ridges. The frequency of hypsometric histograms have been compared to consider major disparities among DEMs.

The Topographic Wetness Index (*TWI*) is a classic indicator which quantifies the effect of topography on hydrological processes (including soil logging) by combining the area contributing to local upslope and slope, it is usually used for quantifying topographical control of hydrological processes. Methods for calculating this index vary mainly in the way the zone contributing upslope is measured. We have calculated the slope and specific watershed area and the Topographic Wetness Index using the SAGA-GIS *TWI* Tool. *TWI* [52] is determined as:

$$TWI = \ln\left(\frac{a}{\tan\beta}\right) \tag{7}$$

where *a* is the local upslope area drains to a certain point per unit contour length, and the local slope is tanβ.

Topographic LS factor represents the topographic erosion susceptibility. The LS factor is defined as the integrated slope length and slope steepness index. The LS factor has been calculated using Universal Soil Loss Equation (USLE) [53], based on slope and (specific) watershed area, as a substitute for slope length. The SAGA-GIS LS tool takes only a Digital Elevation Model (DEM) as input and derives watershed areas according to [54]. The LS factor is defined as:

The slope length factor (*L*):

$$L = \left(\frac{\lambda}{22.13}\right)^{m} \tag{8}$$

where the length of the RUSLE unit plot is 22.13, the slope-length exponent is (m) and the slope-length is (λ).

Slope-length exponent (*m*):

$$m = \frac{\beta}{(1+\beta)} \tag{9}$$

where β is the ratio of rill to interrill erosion.

The slope steepness factor (S):

$$S = 10.8 \sin\theta + 0.03 , S < 9\% \quad (10)$$

$$S = 15.8 \sin\theta + 0.03 , S \geq 9\% \quad (11)$$

where θ is the angle of the slope in degree.

3. Result

3.1. Vertical accuracy assessment and validation of DEMs

The SRTM 3-arc-sec 90 m, ASTER GDEM 1-arc-sec 30 m), SRTMGL1 V003 1-arc-sec 30 m and ALOS-PALSAR 12.5 m DEMs were evaluated against accurate elevation points. To assess and describe the accuracy of the four DEMs, several metrics were applied (Table 1) , including the mean error (Meanerror), Sample Variance (σ2), standard deviation error (STD) and root mean square error (RMSE).

Four scatter plots have been produced and correlation coefficients were determined (Figure 4a–d). Overall, all scatter plots show a perfect fit between reference and DEM elevation values, possibly due to the large number of well distributed reference points. Accordingly, the result obtained for ALOS-PALSAR shows a substantial strong positive correlation with correlation coefficient of r = 0.9995 followed by the correlation coefficient of SRTM 1-arcsec with r = 0.9994, then that of ASTER GDEM with r = 0.9991 and finally SRTM 3-arcsec with r = 0.9981.

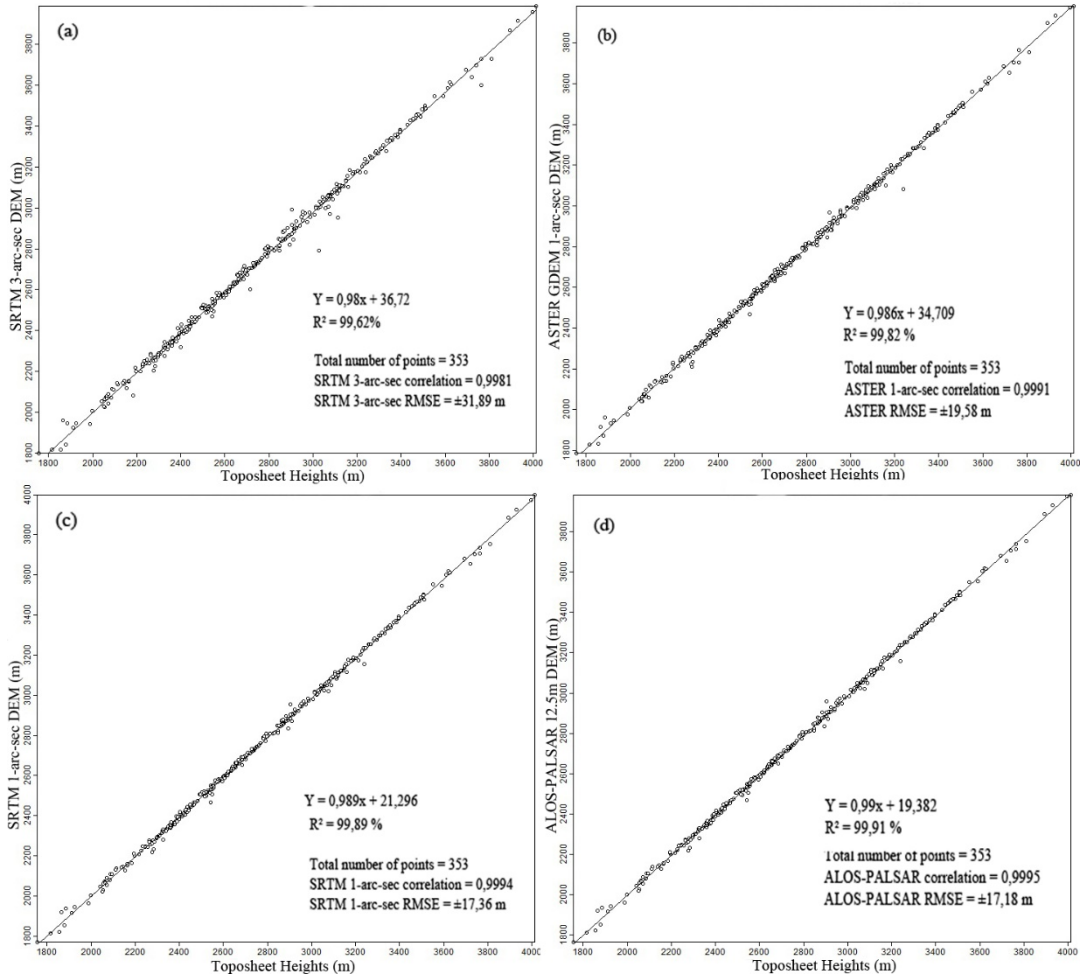

Figure 4. Scatter plots of random points selected from SRTM 3-arcsec DEM (a), ASTER GDEM 1-arcsec DEM (b), SRTM 1-arcsec DEM (c) and ALOS-PALSAR DEM (d) against toposheet elevations showing RMSE of ±31.89 m, ±19.58 m, ±17.39 m and ±17.18 m respectively.

The applied metrics, i.e. the mean error ($Mean_{error}$), Sample Variance (σ^2), standard deviation error (STD) and root mean square error (RMSE) of these selected subsets gave comparable values across the DEMs, generally indicating a good accuracy and a very close similarity between ALOS-PALSAR and SRTM 1-arc-sec. The root mean square error was used for evaluating both random and systematic errors. The USGS adopted this error metric to evaluate DEM products, comparing them with elevation points, which reflect the most likely elevations at particular emplacements. RMSE results are very close when comparing ALOS-PALSAR and SRTM 1-arc-sec DEMs, but rather different from the ASTER 1-arcsec DEM. The SRTM 3-arcsec RMSE was much higher than for the three DEMs used, increasing from ±17.18 m, ±17.39 m, ±19.58 m to ±31.89 m.

The RMSE of all the DEMs for different elevation ranges (Figure 5) shows that the SRTM 30 and ALOS PALSAR 12.5 are the most accurate as shown by the lowest RMSE, while SRTM 90 was the least accurate with the highest RMSE. ASTER 30 gave the lowest RMSE in the 2000–2900 m elevation range. All DEMs were most accurate in the 3800–4100 m elevation range.

These findings support the choice of using ALOS-PALSAR (12.5 m) and SRTM 1-arcsec (30 m) elevation data sets instead of ASTER 1-arcsec (30 m) and SRTM 3-arcsec (90 m) DEMs in our analysis of morphometric parameters.

Table 1. Statistics on the reference elevation values, SRTM 3-arcsec (90 m), ASTER GDEM 1-arcsec (30 m), SRTM 1-arcsec (30 m) and ALOS-PALSAR (12.5 m) DEMs in the study area.

	Toposheet (m)	SRTM (90 m)	ASTER (30 m)	SRTM (30 m)	ALOS-PALSAR (12.5 m)
Min	1754.000	1798.171	1783.890	1768.220	1763.632
Max	4014.000	3988.683	3982.892	4000.286	3982.893
Mean	2761.035	2746.393	2758.604	2753.280	2753.272
$Mean_{error}$	–	14.561	2.338	7.651	7.691
σ^2	–	807.827	379.274	243.625	236.881
Σ	444.639	437.167	438.878	440.149	440.450
RMSE	–	31.899	19.587	17.363	17.186

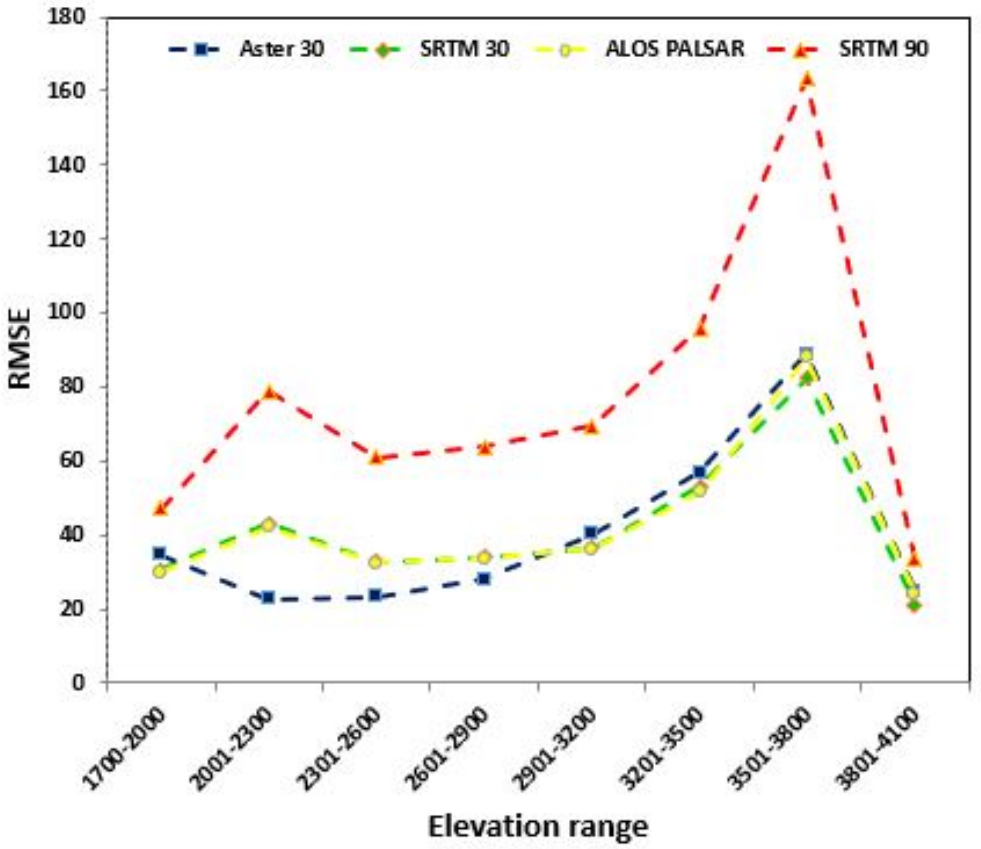

Figure 5. Scatter plots of random points selected from SRTM 3-arcsec DEM (a), ASTER GDEM 1-arcsec DEM (b), SRTM 1-arcsec DEM (c) and ALOS-PALSAR DEM (d) against toposheet elevations showing RMSE of ±31.89 m, ±19.58 m, ±17.39 m and ±17.18 m respectively

3.2. Accuracy assessment of watershed morphometric parameters

The summary statistics for elevation, slope, and LS factor for the four DEMs in the watershed area are presented in Table 2. The maximum elevation was observed in ALOS PALSAR and SRTM 1-arcsec, while the minimum value of the maximum elevation was observed in SRTM 3-arcsec. The elevation standard deviation, however, was highest for SRTM 3-arcsec and lowest for ALOS PALSAR and SRTM 1-arcsec DEMs. The box-plot and detailed statistics comparing the slopes and the LS factor derived from the four DEMs suggest greater sensitivity of the LS factor to the slope range (Figure 6). The average slope and slope range are highest in ALOS PALSAR and lowest in SRTM 3-arcsec, however, SRTM 1-arcsec and ASTER 1-arcsec DEMs show the same average slope. The LS factor values showed ALOS PALSAR to have the highest values, followed by LS factor value obtained using SRTM 1-arcsec while SRTM 3-arcsec gave relatively lowest LS factor values compared to the three DEMs. According to the statistics in Table 3, the watershed morphometric parameters obtained using SRTM 1-arcsec were very comparable to that of the ALOS-PALSAR DEM, followed by ASTER GDEM 1-arcsec. The SRTM 3-arcsec parameters showed a large difference when comparing to the three DEMs.

Table 2. Statistics of DEMs analyzed in the M'Goun watershed.

	SRTM (90 m)	ASTER (30 m)	SRTM (30 m)	PALSAR (12.5 m)
DEM Elevation:				
Min	1442	1432	1436	1434
Max	4031	4037	4054	4057
Mean	2454,74	2458.67	2454.88	2456.10
standard deviation	505.74	505.9	505.6	505.55
Slope:	1.26	1.21	1.41	1.5
Average SLOPE	0.27	0.32	0.32	0.34
LS Factor:	74.29	91.6	125.79	171.53
Average LS FACTOR	5.87	6.47	6.36	6.25

Table 3. M'Goun watershed: morphometric parameters estimated from the four DEMs.

Parameters	SRTM (90 m)	ASTER (30 m)	SRTM (30 m)	PALSAR (12.5 m)
Mean Elevation (m)	2454.74	2458.67	2454.88	2456.10
Elevation Range (m)	2589.00	2605.00	2612.00	2616.00
Mean stream length (km)	48803.81	50171.87	50791.37	50997.91
Maximum stream length (km)	85977.01	88864.81	89403.87	89831.62
Concentration time (h)	7.89	8.17	8.22	8.26
Equivalent Rectangle (A)	123409.69	128443.17	129936.53	134755.96
Equivalent Rectangle (B)	5004.52	4824.78	4803.98	4644.04
Orographic coefficient	48.78	48.77	48.27	48.20
Massivity coefficient	2.08	2.15	2.16	2.23

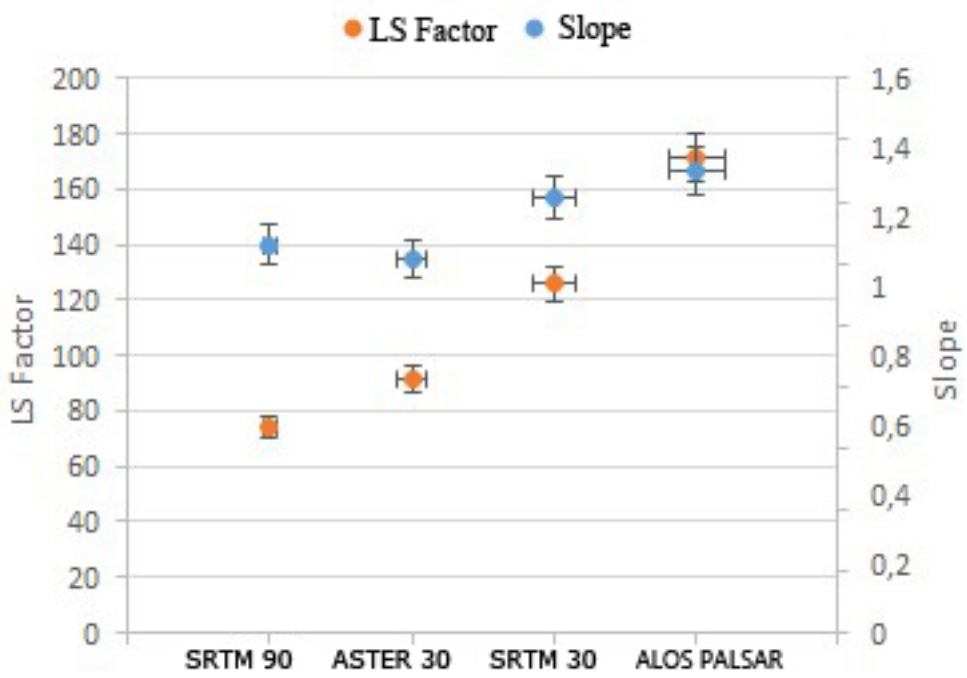

Figure 6. Box-plot of the Slope and LS Factor of DEMs in M'Goun watershed.

3.3. Comparison of the erosion related topographic indices

3.3.1. Elevation profiles

It appears that the A–B cross-section of the four DEMs f are dissimilar, especially for SRTM 3-arc-sec that shows the largest variation in the elevation profile distinctly at high altitude and in valleys (Figures 7 and 8). SRTMGL1 V003 1-arcsec and ALOS-PALSAR showed approximately similar elevation profiles at high to moderate altitude, steep slopes, and valleys. The ASTER GDEM 1-arcsec profile was consistently different from that of SRTMGL1 V003 1-arcsec and ALOS-PALSAR DEMs, and elevation in the higher areas and valleys was overestimated. This difference in ASTER can be explained by the smoothing process in stereo-correlation [55] and the impact of rugged relief and deep valleys on stereoscopic DEM's performance [56]. A visual inspection of Figure 8 reveals that the SRTMGL1 V003 1-arcsec is closer to the ALOS-PALSAR than to ASTER GDEM. This further confirms that SRTMGL1 V003 1-arcsec has an accuracy superior to ASTER GDEM 1-arcsec and SRTM 3-arcsec.

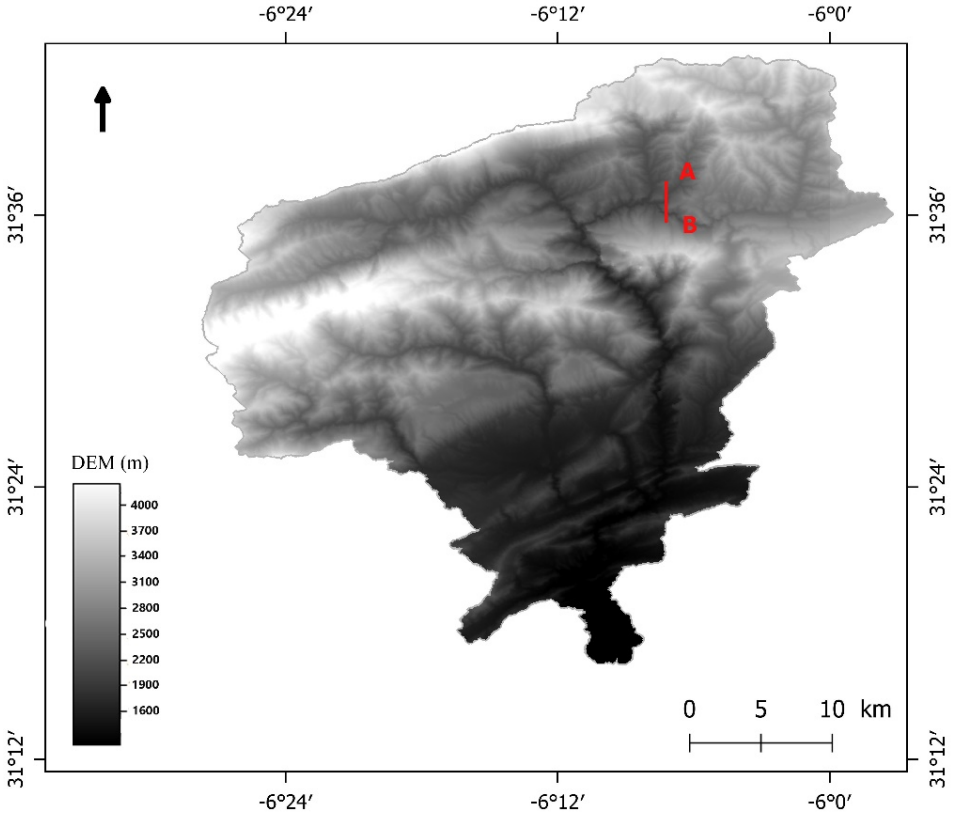

Figure 7. Digital Elevation Model ALOS PALSAR (12.5 m): location of section A–B in the study area.

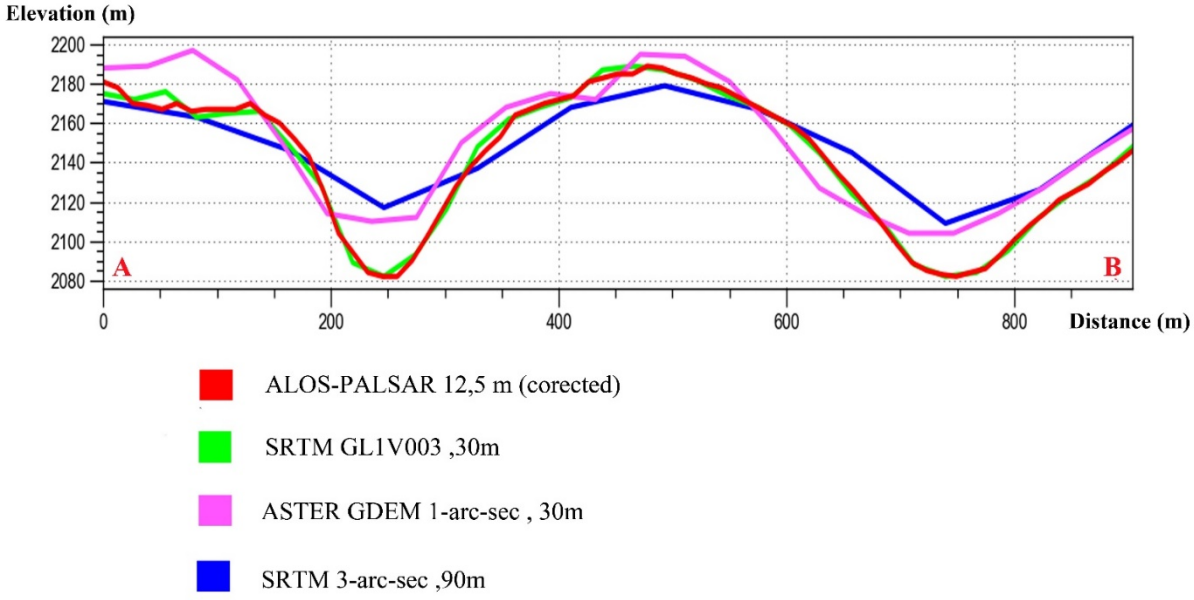

Figure 8. Elevation profiles of all DEMs along the A–B section l in Figure 7.

3.3.2. Hypsometry

A watershed basin's hypsometric curve (area-altitude relationship) demonstrate the relative ratio of the catchment area at or above a given height relative to the total watershed relief [57]. For the four DEMs, hypsometric curves have the same shape and the histograms are bimodal and show two classes of altitude more frequent than the others (Figure 9) with the peak values in the range 2400–2600 m in all DEMs.

This resemblance proves the analogous representation given by the four DEMs. The main difference between the four histograms is the number of pixels in each DEM within the same region. The histograms are almost identical and show several modal classes except that the distribution of altitude classes of the DEM ALOS PALSAR is the most homogeneous (Figure 9d) while that of the DEM SRTM 3-arcsec shows a lot of heterogeneity (Figure 9a).

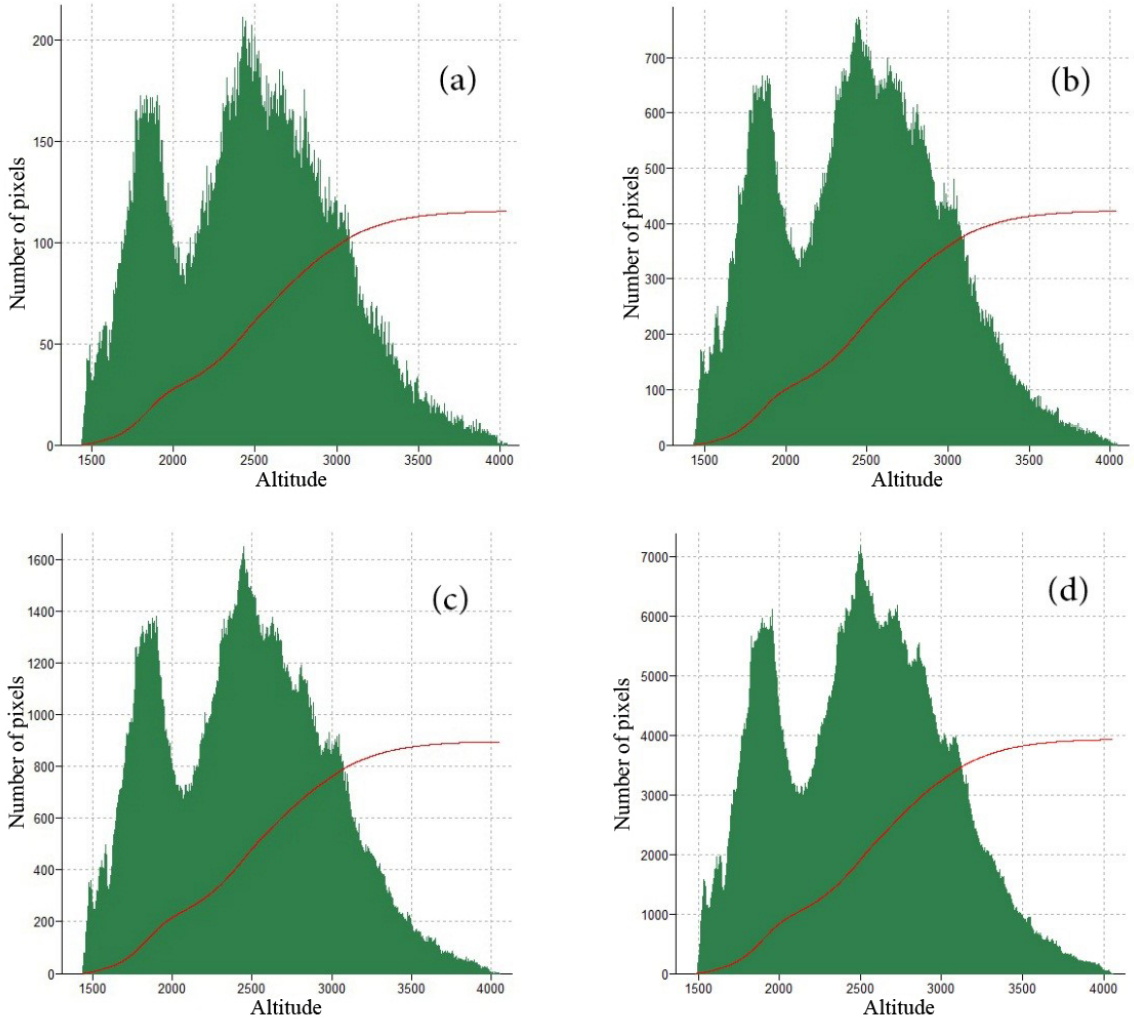

Figure 9. Hypsometric histograms and cumulative curves of the distribution of altitude classes for each DEM, (a) SRTM 3-arcsec 90 m, (b) ASTER GDEM 1-arcsec 30 m, (c) SRTMGL1 V003 1-arcsec 30 m, (d) ALOS PALSAR 12.5 m.

3.3.3. Topographic wetness index (TWI)

In order to assess the impact of the spatial resolution on topographical indices relevant to the water erosion risk in the Wadi M'Goun watershed, the topographic wetness index extracted from the four DEMs in the M'Goun watershed has been used in this study, not as a test for DEMs but to make a comparison between different TWI maps resulting from the four DEMs. The topographic wetness index (TWI) maps obtained with the four DEMs (Figure 10a–d) measure topographical effects on hydrological processes. Roughly, TWI shows high values, associated with relatively wetter areas, especially in the valley of the main stream. In more detail, some other areas characterized by high differences in TWI values can be noticed, with the differences were concentrated where the slope of the landscape is gentle or flat. SRTM 3-arc-sec DEM gives a general view about TWI and when compared with the other DEMs, great differences are visible along the watershed. Particularly interesting are the areas downstream in the southwest and the northern part of the basin. The SRTM 1-arc-sec and ASTER 1-arc-sec DEMs present different features, The largest discrepancies being observed in the channel network, where the TWI hits the highest values in the SRTM 1-arc-sec DEM. This shows how the same terrain can yield different results when using different DEMs. The TWI maps obtained by ALOS-PALSAR 12.5 m and SRTM 1-arc-sec look similar and give detailed, high resolution TWI maps.

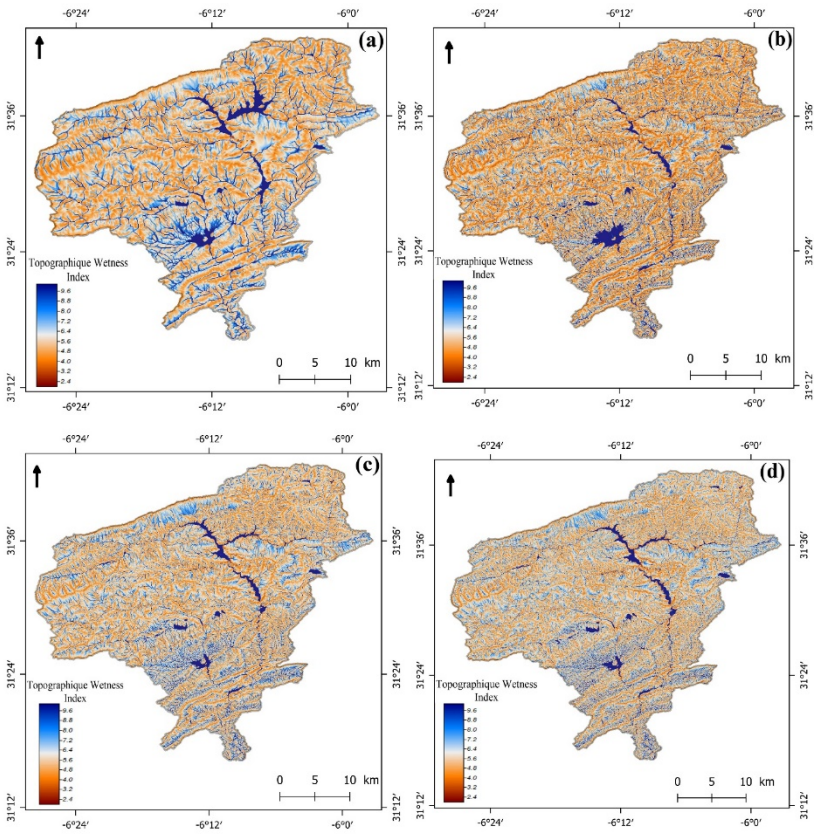

Figure 10. Topographic Wetness Index maps: (a) SRTM 3-arcsec 90 m, (b) ASTER GDEM 1-arcsec 30 m, (c) SRTMGL1 V003 1-arcsec 30 m, (d) ALOS PALSAR 12.5 m.

3.3.4. Topographic factor (LS)

The topographic factor (LS), depends on both slope length and slope inclination. The LS factor data of the Wadi M'Goun watershed were generated using the SAGA GIS. First, we use the DEM to calculate the slope, then the orientation and the cumulative length of the slope and finally the LS factor.

The LS factor is a variable in the calculation of soil erosion. The variation within each DEM is used to evaluate the effect of DEM accuracy on estimated soil erosion. Before analyzing the LS factor of the M'Goun watershed, a general area assessment was conducted by merging all DEMs LS retrievals from 0 to 24 into 1 LS class (Figures 11 and 12). The LS factor is higher in the northern, north-west and central areas, where the elevation and slope are high, while it is low in the southern part. In the SRTM 3 arc-seconds file little variation in LS factor is identified due to the lower DEM spatial resolution. It should be noted that lower LS values suggest a lower erosion risk, although due to the lower spatial resolution. ASTERGDEM 1-arcsec, SRTM 1-arcsec and ALOS-PALSAR 12.5 m give us more detailed information about zones with erosion risk, and the difference between them can be seen when considering areas with low risk of erosion (Figure 11). It is found that the results obtained by SRTM 1-arcsec and PALSAR 12.5 m are almost identical, the LS accuracy increase when the spatial resolution of DEMs increase, moving progressively from SRTM 3-arc-sec to ALOS PALSAR 12.5 m. The high spatial resolution gives results comparable to reality on the field. These results are in agreement with [58] who show the effect of DEM accuracy and resolution on topographic indices. They reported that the high-precision and high-resolution DEM offers the capability to improve the quality of topographic indices extracted from DEMs.

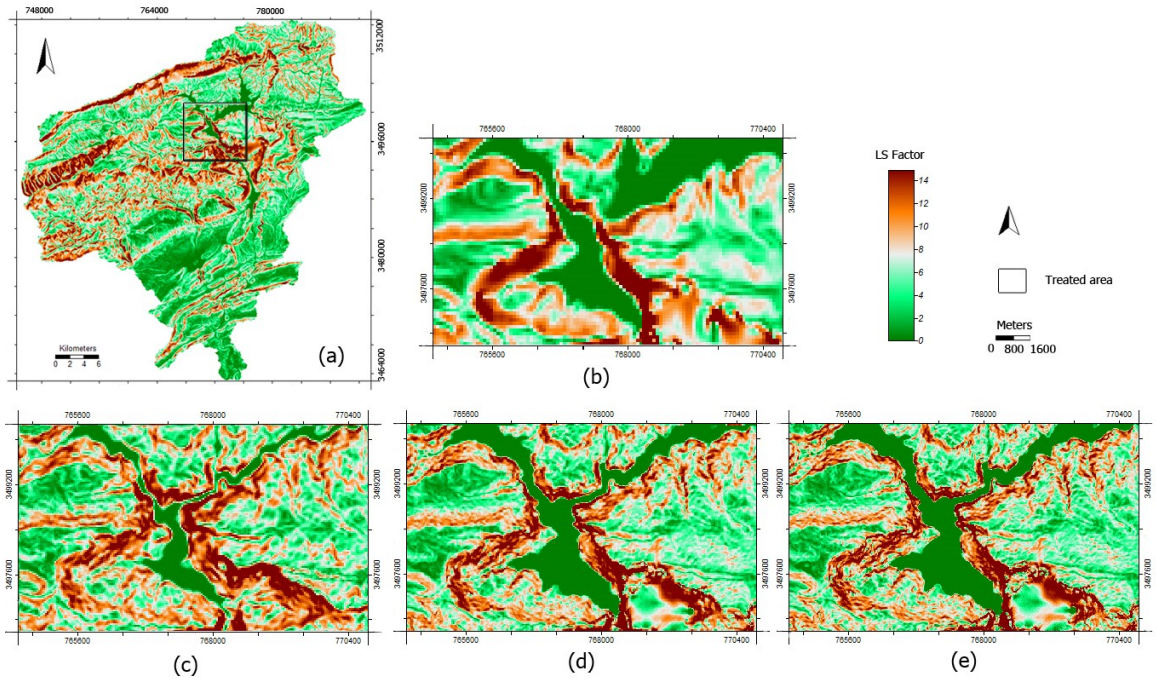

Figure 11. (a) Map of topographic factor LS in M'Goun watershed, (b) SRTM 3-arcsec 90 m, (c) ASTER GDEM 1-arcsec 30 m, (d) SRTMGL1 V003 1-arcsec 30 m, (e) ALOS PALSAR 12.5 m.

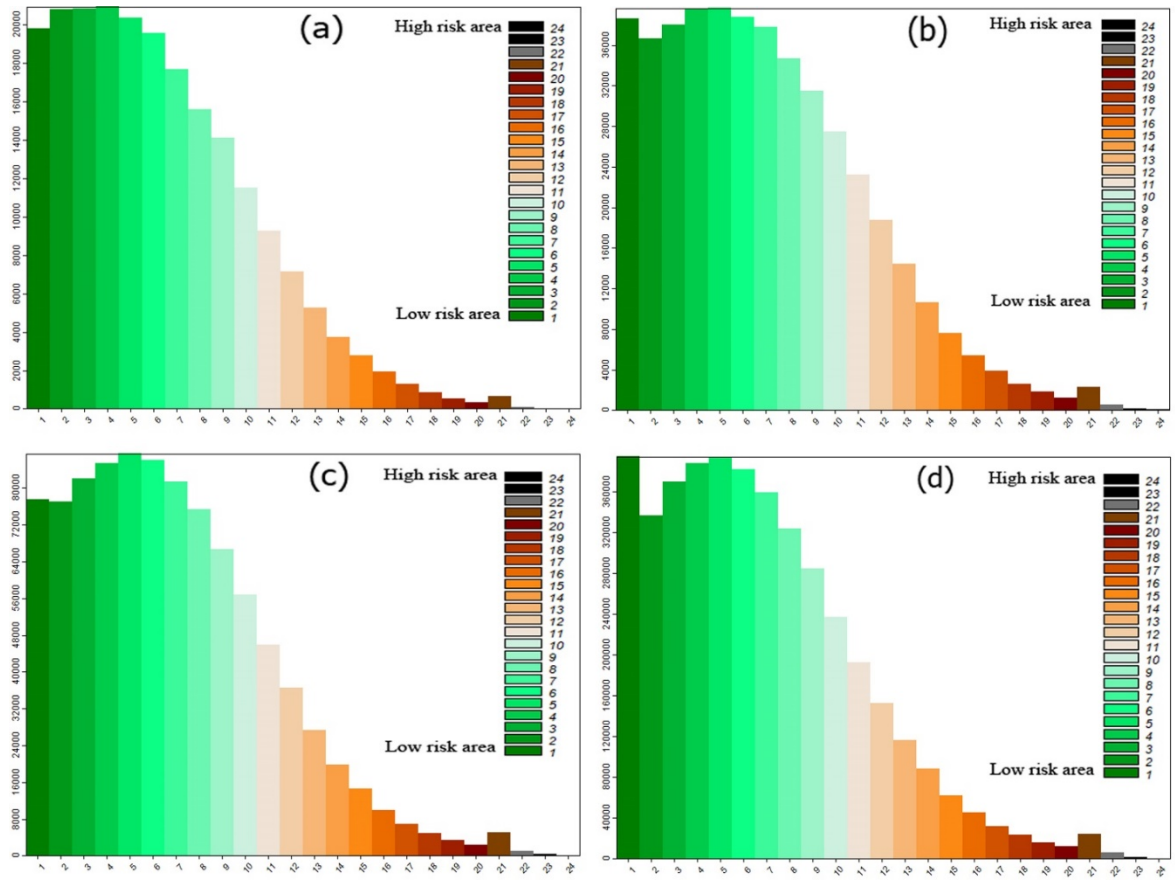

Figure 12. Histograms of LS representing the rate of water erosion risk of each DEM: (a) SRTM 3-arcsec 90 m, (b) ASTER GDEM 1-arcsec 30 m, (c) SRTMGL1 V003 1-arcsec 30 m, (d) ALOS PALSAR 12.5 m.

3.3.5. Vulnerability to water erosion

The superposition of the different maps resulting from different indices and factors, using the open source SAGA GIS, allowed us to create a map that delineates the zones potentially vulnerable to water erosion. To assess the impact of the difference in accuracy across the four DEMs on our assessment of vulnerability to water erosion, we have chosen arbitrarily a small zone in the M'Goun watershed (Figure 13a). High-risk zones are situated in the upstream and central parts of the basin, characterized by high altitudes, steep slopes, intense fracturing, bare soils, and carbonate or carbonato-evaporitic lithology. In the downstream part it is rather the presence of the Cretaceous, Eocene and Paleocene cliffs, which favors landslides and soil degradation under the effect of water erosion. These erosion maps highlight areas most sensitive to erosion. It is, therefore, possible to establish land management interventions to mitigate the vulnerability of the most fragile areas threatened by erosion.

The histograms resulting from the four DEMs of different resolutions show the same classes (Figure 13b). For the blue classes with a low erosion rate, all DEMs have almost the same percentage, except the 3-arc-sec SRTM, which has a slightly lower value than the other DEMs. Concerning the classes that present an average risk of erosion, estimated soil erosion rate depends on the DEMs resolution and the SRTM 1-arc-sec and ASTER 1-arc-sec, which have the identical resolution, show

almost the same percentage. The SRTM 3-arcsec does not give detailed results on zones with erosion risk in view of the low spatial resolution, contrary to the ALOS-PALSAR DEM, which shows the ability to outline the erosion risk zones reasonably accurately due to the decrease of the grid space DEM. About the high erosion risk, SRTM 3-arcsec DEM does not give good quality of mapping and delineating the high erosion rate areas, SRTM 1-arcsec and ASTER 1-arcsec show almost similar results, while the ALOS PALSAR DEM for all classes gives detailed information about the areas of high soil erosion rate. Consequently, the estimated rate of erosion decreases due to the decrease in the values of the LS factor. In the same way, low soil erosion estimates for SRTM 3-arcsec DEM are due to low mean elevation, slope, and LS values compared to SRTM 1-arcsec, ASTER GDEM 1-arcsec, and ALOS PALSAR.

a

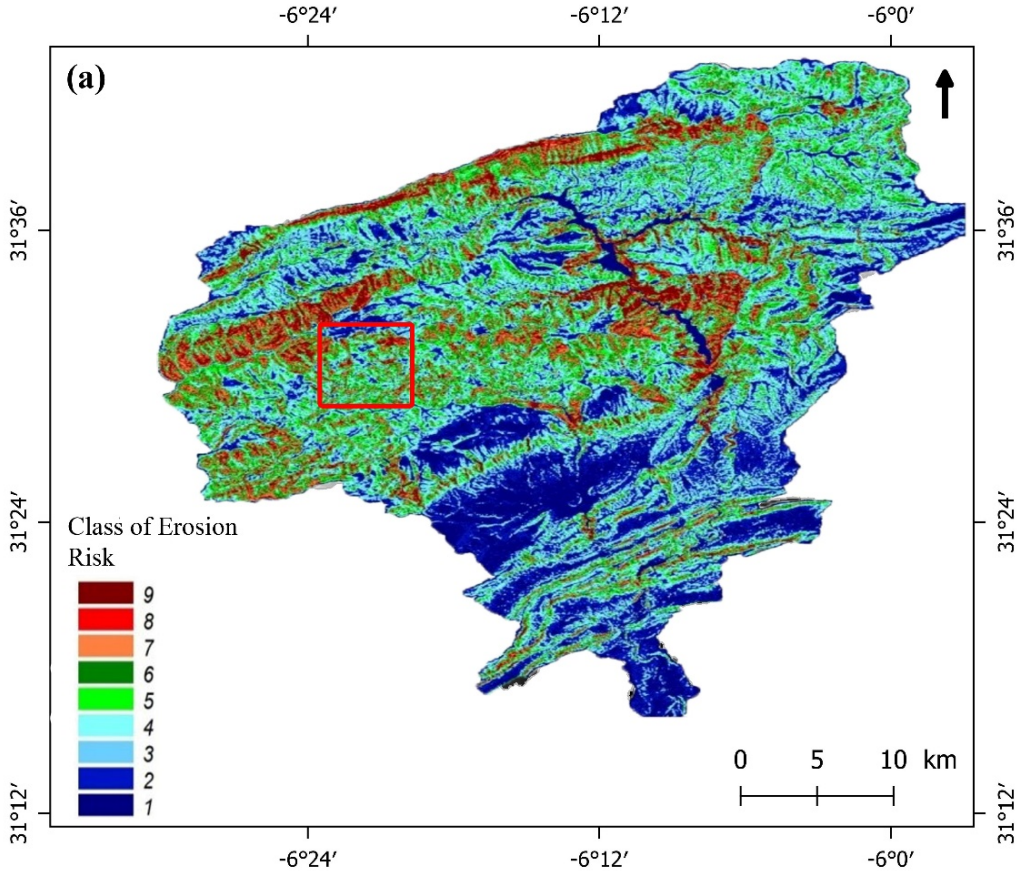

Figure 13. (a) Water erosion risk map of M'Goun watershed, (b) Erosion maps and histograms represent the rate of water erosion risk in a limited zone of M'Goun watershed resulting from ALOS-PALSAR, SRTMGL1 V003 1-arcsec, SRTM 3-arcsec, ASTER GDEM 1-arcsec.

b

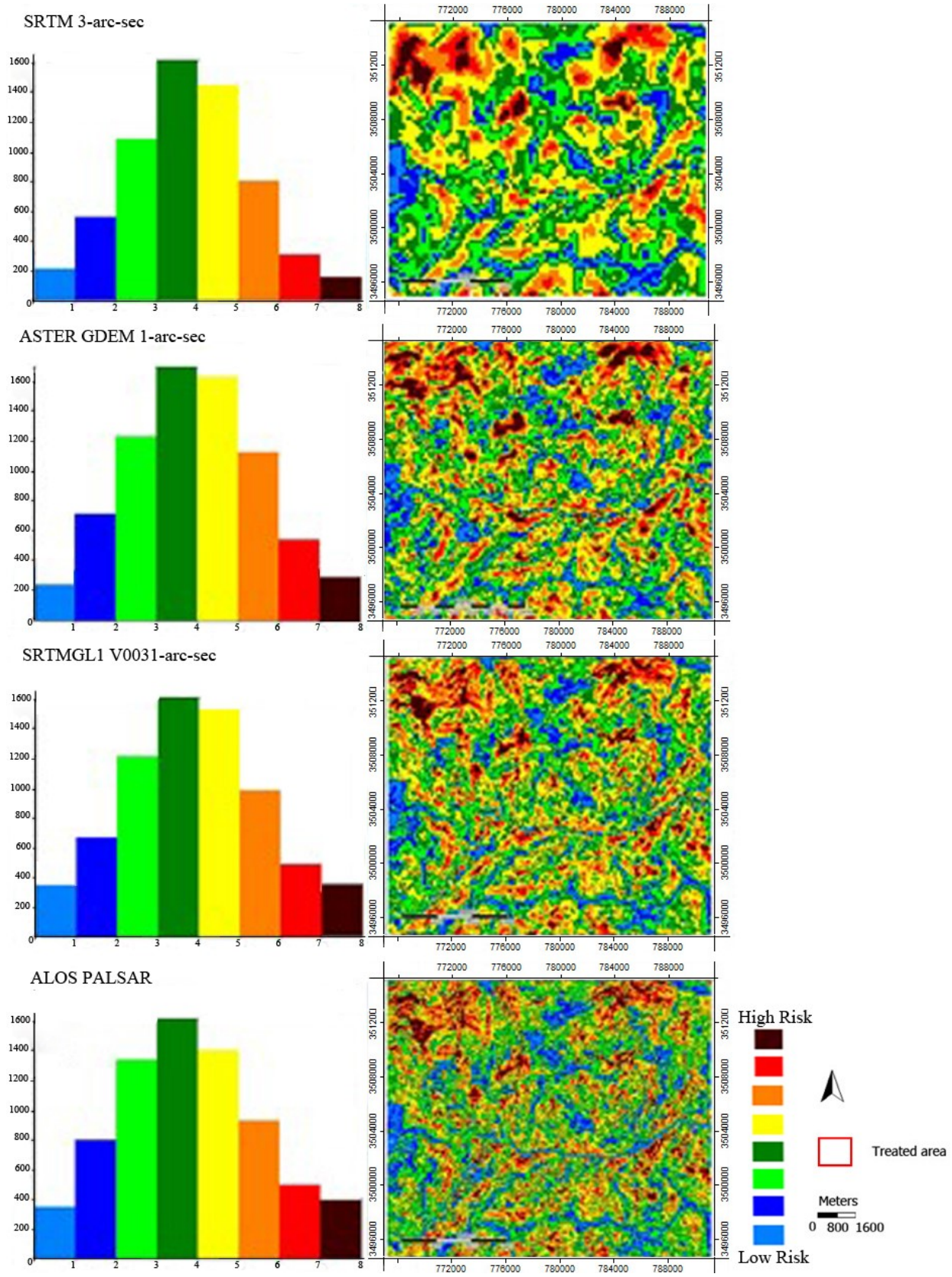

Figure 13. *Continued.*

4. Discussion

The results of the evaluation of the four DEMs demonstrate that major variations exist between the morphometric parameters and the topographical indices extracted from the four DEMs. These dissimilarities underline that the selection of DEM has a significant impact on topographical and morphometric indices and thus on the risk assessment of water erosion in mountainous regions, [56] have validated this by comparing topographical parameters relevant to estimate erosion risk from SRTM and ASTER DEMs. The variance in the risk of water erosion in different parts of the Wadi M'Goun watershed is very prominent, where the four DEMs give a higher water erosion risk at high altitudes and LS factor which are located in the northern, north-west and central areas (Figure 13a). Distribution of erosion rate of ALOS PALSAR 12.5 m is more important regarding the clarity of areas susceptible to water erosion, the number of grid cells in each class and the delimitation of zones with high risk, unlike the low-resolution DEM SRTM 3-arcsec which presents the erosion rate quite generalized and give less detailed delineation of different erosion classes, SRTM 1-arcsec 30 m and ASTER GDEM 1-arcsec 30 m show a similar pattern (Figure 13b).

Terrain morphology is one of the major determinants of DEM accuracy. The terrain in the M'Goun watershed is complex, with large drainage networks and elevations ranging from 1400 to over 4000 meters, therefore this area is an ideal zone to evaluate a DEM accuracy. The elevation variance can be a terrain roughness measure, with a large variance being an indicator of elevated variability in elevation [59]. ALOS PALSAR and SRTM 1-arcsec DEMs seem to demonstrate similarities with respect to the degree of local deviations, only these deviations were the lowest for ALOS PALSAR relative to the reference measurements. Although studies on such evaluations in rugged mountain terrain have been very limited e.g. [56], these elevated RMSE values can be regarded as a consequence of the extremely complex terrain that is a widespread feature in the Central High Atlas mountains.

Many projects have been carried out to evaluate the vertical accuracy of various DEMs in mountainous regions [23,25,32,35,60], but only rare cases of DEM accuracy were described in the literature using field data e.g. [56]. The mean differences between ALOS PALSAR TOPO, SRTM 30 m TOPO, ASTER TOPO, and SRTM 90 m TOPO DEMs are quite large, focusing on the absolute elevation difference between DEMs. These differences are highly compatible, however, with the latest results based on reference topographical maps, which gave RMSE on elevation between 15 m and 70 m [10,17,56,60].

The comparison of topographical indicators of erosion risk derived from the four DEMs highlights the good performance of ALOS PALSAR and SRTM 1-arcsec, as shown by the clear delineation of areas susceptible to water erosion. On the other hand, ASTER 1-arcsec does not provide appropriate and precise topographical details to assess erosion risk at high elevation. A similar observation was mentioned by [61,56], when errors were observed in calculations of the upslope area, the erosion rates were underestimated due to the complex terrain as captured by the high-resolution ASTER DEM.

ALOS PALSAR and SRTM 1-arcsec DEMs has been found to be the most performance of the examined DEMs and, given the availability of open sources and the least processing costs and time requirements of these DEMs, they can be considered the most appropriate of the tested DEMs for the study of the watershed at high altitude [32,62].

5. Conclusion

We have evaluated four of the up-to-date and open-sources digital elevation models against accurate ground truth information in the M'Goun watershed using DEMs at different spatial resolution: SRTM 3-arcsec, SRTMGL1 V003 1-arcsec, ASTER GDEM 1-arcsec, and ALOS PALSAR. The conversion of DEMs into the same datum is a critical step prior to assess their accuracy. DEM with the highest resolution (ALOS PALSAR 12.5 m) gave the best performances with lower uncertainty and their horizontal and vertical accuracies are excellent compared to DEMs with low resolution. As regards the DEMs with the same 30 m resolution, results show that SRTM 1-arcsec carry out better than ASTER GDEM 1-arcsec. At this higher spatial resolution, as well as SRTM 1-arcsec performs better [32,63,64]. The SRTM 3-arcsec DEM gave the worst accuracy compared with the three other DEMs. The ALOS-PALSAR DEM is more accurate to evaluate water erosion vulnerability in a high elevation watershed, the increase of spatial resolution leads to the clarity of erosion factor and of the delimitation of vulnerable areas to water erosion risk. The only issue is that the DEM data at this resolution and extent often need a geoid correction with a method that consists in determining by GPS the ellipsoidal height of some benchmarks and leveling the altitude at the same points. The results obtained improve the effect of DEM accuracy and resolution on topographic indices. Note that lower LS values indicate a lower erosion, however, the estimated rate of erosion decreases due to the decrease in the values of the LS factor. Consequently, low soil erosion estimates for DEMs are due to low derived values of mean elevation, slope, and LS factor. It should be noted that the DEMs with high accuracy and high resolution, ALOS PALSAR 12.5 m, and SRTM 1-arc-sec, offer the capacity of improving the quality of topographic indices extracted from DEMs. Possibly the results obtained differ in diverse study areas, but DEMs with higher accuracy (ALOS-PALSAR, SRTMGL1 V003 1-arcsec) will offer more precise outcomes and decrease the uncertainty. This study is an effort to demonstrate and analyze the uncertainties introduced by freely DEMs in the accuracy assessment of water erosion risk to acquaint the researchers with the use of up-to-date open-source DEMs. We hope that this paper provides a reference to choose open source DEMs with higher accuracy for natural hazards assessment.

Acknowledgments

Authors would like to gratefully acknowledge the United States Geological Survey (USGS), The Ministry of Economy, Trade, and Industry (METI) of Japan and the NASA, and JAXA, for their insights and support through data sharing platforms.

Conflict of interest

The authors declare no conflict of interest.

References

1. Forsberg R (1984) A study of terrain reductions, density anomalies and geophysical inversion methods in gravity field modelling. No. OSU/DGSS-355, Ohio State University.

2. Müller-wohlfeil DI, lahmer W, krysanova V, et al. (1996) Topography-based hydrological modeling in the Elbe River drainage basin. In: Third International Conference/Workshop on Integrating GIS and Environmental Modeling, National Center for Geographic Information and Analysis, C.A, Santa Fe.
3. Mark DM, Smith B (2004) A science of topography: from qualitative ontology to digital representations. In: Bishop MP, Shroder JF (Eds.), *Geographic Information Science and Mountain Geomorphology*, Springer–Praxis, Chichester, England, 75–97.
4. Khal M, Algouti Ab, Algouti A (2018) Modeling of Water Erosion in the M'Goun Watershed Using OpenGIS Software. In: World Academy of Science, Engineering and Technology International Journal of Computer and Systems Engineering, 12: 1102–1106.
5. Mcluckie D, NFRAC (2008) Flood risk management in Australia. *Aust J Emerg Manag* 23: 21–27.
6. Ait Mlouk M, Algouti Ab, Algouti Ah, et al. (2018) Assessment of river bank erosion in semi-arid climate regions using remote sensing and GIS data: a case study of Rdat River, Marrakech, Morocco. *Estud Geol* 74: 81.
7. Williams J (2009) Weather Forecasting. *The AMS Weather Book: The Ultimate Guide to America's Weather*. American Meteorological Society, Boston, MA.
8. Da ros D, Borga M (1997) Use of digital elevation model data for the derivation of the geomorphological instantaneous unit hydrograph. *Hydrol Process* 11: 13–33.
9. Tesfa TK, Tarboton DG, Watson DW, et al. (2011) Extraction of hydrological proximity measures from DEMs using parallel processing. *Environ Model Softw* 26: 1696–1709.
10. Jobin T, Prasannakumar V (2015) Comparison of basin morphometry derived from topographic maps, ASTER and SRTM DEMs: an example from Kerala, India. *Geocarto Int* 30: 346–364.
11. Kishan SR, Anil KM, Vinay KS, et al. (2012) Comparative evaluation of horizontal accuracy of elevations of selected ground control points from ASTER and SRTM DEM with respect to CARTOSAT-1 DEM: a case study of Shahjahanpur district, Uttar Pradesh, India. *Geocarto Int* 28: 439–452.
12. Tian Y, Lei S, Bian Z, et al. (2018) Improving the Accuracy of Open Source Digital Elevation Models with Multi-Scale Fusion and a Slope Position-Based Linear Regression Method. *Remote Sens* 10: 1861.
13. Cuartero A, Felicsimo AM, Ariza FJ (2004) Accuracy of DEM generation from TERRA-ASTER stereo data. *Int Arch Photogramm Remote Sens* 35: 559–563.
14. Day T, Muller J (1988) Quality assessment of digital elevation models produced by automatic stereo-matchers from SPOT image pairs. *Photogramm Rec* 12: 797–808.
15. Fujisada H (1994) Overview of ASTER instrument on EOS-AM1 platform. In: Proceedings of SPIE, 2268: 14–36.
16. Toutin T (2008) ASTER DEMs for geomatic and geoscientific applications. *Int J Remote Sens* 29: 1855–1875.
17. Bolstad PV, Stowe T (1994) An evaluation of DEM accuracy: elevation, slope, and aspect. *Photogramm Eng Remote Sens* 60: 1327–1332.
18. Blöschl G, Sivapalan M (1995) Scale issues in hydrological modelling: A review. *Hydrol Process* 9: 251–290.

19. Vijith H, Seling LW, Dodge-Wan D (2015) Comparison and Suitability of SRTM and ASTER Digital Elevation Data for Terrain Analysis and Geomorphometric Parameters: Case Study of Sungai PatahSubwatershed (Baram River, Sarawak, Malaysia). *Environ Res Eng Manag* 71: 23–35.
20. Beven KJ, Moore ID (1993) Terrain analysis and distributed modelling in hydrology. New York: Wiley.
21. Wang XH, Yin ZY (1998) A comparison of drainage networks derived from digital elevation models at two scales. *J Hydrol* 210: 221–241.
22. Wang W, Yang X, Yao T (2012) Evaluation of ASTER GDEM and SRTM and their suitability in hydraulic modelling of a glacial lake outburst flood in southeast Tibet. *Hydrol Process* 26: 213–225.
23. Nikolakopoulos KG, Kamaratakis EK, Chrysoulakis N (2006) SRTM vs ASTER elevation products. Comparison for two regions in Crete, Greece. *Int J Remote Sens* 27: 4819–4838.
24. Pryde JK, Osorio J, Wolfe ML, et al. (2007) USGS. An ASABE Meeting Presentation Paper Number: 072093, Minneapolis Convention Center Minneapolis, Minnesota, June; 072093.
25. Jing C, Shortridge A, Lin S, et al. (2014) Comparison and validation of SRTM and ASTER GDEM for a subtropical landscape in Southeastern China. *Int J Digit Earth* 7: 969–992.
26. Dewitt JD, Warner TA, Conley JF (2015) Comparison of DEMS derived from USGS DLG, SRTM, a statewide photogrammetry program, ASTER GDEM and LiDAR: implications for change detection. *GIScience Remote Sens* 52: 179–197.
27. Moudrý V, Lecours V, Gdulová K, et al. (2018) On the use of global DEMs in ecological modelling and the accuracy of new bare-earth DEMs. *Ecol Modell* 383: 3–9.
28. Zhang K, Gann D, Ross M, et al. (2019) Comparison of TanDEM-X DEM with LiDAR Data for Accuracy Assessment in a Coastal Urban Area. *Remote Sens* 11: 876.
29. Kinsey-Henderson AE, Wilkinson SN (2012) Evaluating Shuttle radar and interpolated DEMs for slope gradient and soil erosion estimation in low relief terrain. *Environ Modell Softw* 40: 128–139.
30. Lin S, Jing C, Coles NA, et al. (2013) Evaluating DEM source and resolution uncertainties in the Soil and Water Assessment Tool. *Stoch Environ Res Risk Assess* 27: 209–221.
31. Williams JR, Berndt HD (1977) Sediment yield prediction based on watershed hydrology. Transactions of the American Society of Agricultural and Biological Engineers. *Trans ASAE* 20: 1100–1104.
32. Rexer M, Hirt C (2014) Comparison of free high-resolution digital elevation data sets (ASTER GDEM2, SRTM v2.1/v4.1) and validation against accurate heights from the Australian National Gravity Database. *Aust J Earth Sci* 61: 213–226.
33. Renard KG, Foster GR, Weesies GA, et al. (1997) Predicting soil erosion by water: a guide to conservation planning with the revised universal soil loss equation (RUSLE). *Agriculture Handbook*, U.S. Department of Agriculture, No 703, 404.
34. Prasuhn V, Liniger H, Gisler S, et al. (2013) A high-resolution soil erosion risk map of Switzerland as strategic policy support system. *Land Use Policy* 32: 281–291.
35. Mondal A, Khare D, Kundu S, et al. (2016) Uncertainty of soil erosion modelling using open source high resolution and aggregated DEMs. *Geosci Front* 8: 425–436.
36. Mondal A, Khare D, Kundu S (2017) Uncertainty analysis of soil erosion modelling using different resolution of open-source DEMs. *Geocarto Int* 32: 334–349.

37. Uhlemann S, Thieken AH, Merz B (2014) A quality assessment framework for natural hazard event documentation: application to trans-basin flood reports in Germany. *Nat Hazards Earth Syst Sci* 14: 189–208.
38. USGS (2006) Earth Resources Observation and Science. Available from: https://www.usgs.gov/centers/eros.
39. Wang L, Liu H (2006) An efficient method for identifying and filling surface depressions in digital elevation models for hydrologic analysis and modelling. *Int J Geogr Inf Sci* 20: 193–213.
40. Das A, Agrawala R, Mohan S (2015) Topographic correction of ALOS-PALSAR images using InSAR-derived DEM. *Geocarto Int* 30: 145–153.
41. Jäger R, Kaminskis J, Balodis J (2012) Determination of Quasi-geoid as Height Component of the Geodetic Infrastructure for GNSS-Positioning Services in the Baltic States. *Latv J Phys Tech Sci* 49: 2.
42. Ghilani CD, Wolf PR (2006) *Adjustment Computations: Spatial Data Analysis*, 4th Edition, John Wiley & Sons, Hoboken.
43. Al-Fugara A (2015) Comparison and Validation of the Recent Freely Available DEMs over Parts of the Earth's Lowest Elevation Area: Dead Sea, Jordan. *Int J Geosci* 6: 1221–1232.
44. Shaw EM (1988) Van Nostrand Reinhold International, London, United Kingdom. Hydrology in practice.
45. Strahler AN (1964) Quantitative geomorphology of drainage basin and channel network. In Chow VT (ed), *Handbook of Applied Hydrology*, McGrawHill, NewYork, NY, USA.
46. Wanielista MP, Kersten R, Eaglin R (1997) *Hydrology: Water Quantity and Quality Control*, Wiley, New York.
47. Musy A (2001) Ecole Polytechnique Fédérale, Lausanne, Suisse, e-drologie.
48. Roche M (1963) *Hydrologie de Surface*. Gauthier-Villars, Paris, 140: 659.
49. Horton RE (1945) Erosional development of streams and their drainage basins: hydro physical approach to quantitative morphology. *Geol Soc Am Bull* 56: 275–370.
50. Strahler AN (1952) Hypsometric analysis of erosional topography. *Bull Geol Soc Am* 63: 1117–1142.
51. Schumm SA (1956) Evolution of drainage systems and slopes in badlands at perth amboy, new jersey. *Geol Soc Am Bull* 67: 597–646.
52. Beven KJ, Kirkby MJ (1979) A physically based, variable contributing area model of basin hydrology. *Hydrol Sci Bull* 24: 43–69.
53. Pandey A, Chowdary VM, Mal BC (2007) Identification of critical erosion prone areas in the small agricultural watershed using USLE, GIS and remote sensing. *Water Resour Manage* 21: 729–746.
54. Freeman TG (1991) Calculating Catchment Area With Divergent Flow Based on a Regular Grid. *Comput Geosci* 17: 413–422.
55. Kamp U, Bolch T, Olsenholler J (2005) Geomorphometry of Cerro Sillajhuay (Andes, Chile/Bolivia): Comparison of digital elevation models (DEMs) from ASTER remote sensing data and contour maps. *Geocarto Int* 20: 23–33.
56. Datta PS, Schack-Kirchner H (2010) Erosion Relevant Topographical Parameters Derived from Different DEMs—A Comparative Study from the Indian Lesser Himalayas. *Remote Sens* 2: 1941–1961.

57. Luo W (1998) Hypsometric analysis with a geographic information system. *Comput Geosci* 24: 815–821.
58. Vaze J, Teng J, Spencer G (2010) Impact of DEM accuracy and resolution on topographic indices. *Environ Modell Softw* 25: 1086–1098.
59. Holmes KW, Chadwick OA, Kyriankidis PC (2000) Error in USGS 30-meter digital elevation model and its impact on terrain modelling. *J Hydrol* 233: 154–173.
60. Huggel C, Schneider D, Miranda PJ, et al. (2008) Evaluation of ASTER and SRTM DEM data for lahar modelling: A case study on lahars from Popocatépetl volcano, Mexico. *J Volcanol Geotherm Res* 170: 99–110.
61. De Vente J, Poesen J, Govers G, et al. (2009) The implications of data selection for regional erosion and sediment yield modelling. *Earth Surf Process Landf* 34: 1994–2007.
62. Nitheshnirmal S, Thilagaraj P, Abdul Rahaman S, et al. (2019) Erosion risk assessment through morphometric indices for prioritisation of Arjuna watershed using ALOS-PALSAR DEM. *Model Earth Syst Environ* 5: 907–924.
63. Bhakar R, Srivastav SK, Punia M (2010) Assessment of the relative accuracy of aster and SRTM digital elevation models along irrigation channel banks of Indira Gandhi Canal. *J Water Land-use Manage* 10: 1–11.
64. Hasan A, Pilesjo P, Persson A (2011) The use of LIDAR as a data source for digital elevation models—a study of the relationship between the accuracy of digital elevation models and topographical attributes in northern peatlands. *Hydrol Earth Syst Sci Discuss* 8: 5497–5522.

AIMS Press